Analysis of Glutamate Agonist LY404,039 at Dopamine Receptor D2 Dimeric Models Using Multiscale Molecular Modeling Approaches

Ramin Ekhteiari Salmas[1]*, Philip Seeman[2], Busecan Aksoydan[1], Ismail Erol[1,3], Isik Kantarcioglu[1], Matthias Stein[4], Mine Yurtsever[5], Serdar Durdagi[1]*

[1]Computational Biology and Molecular Simulations Laboratory, Department of Biophysics, School of Medicine, Bahcesehir University, Istanbul, Turkey
[2]Departments of Pharmacology and Psychiatry, University of Toronto, 260 Heath Street West, Unit 605, M5P 3L6, Toronto, Ontario, Canada
[3]Department of Chemistry, Gebze Technical University, Kocaeli, Turkey
[4]Max-Planck Institute for Dynamics of Complex Technical Systems, Molecular Simulations and Design Group, Sandtorstrasse 1, 39106, Magdeburg, Germany
[5]Department of Chemistry, Istanbul Technical University, Istanbul, Turkey

***Corresponding Authors:**

Ramin Ekhteiari Salmas, Ph.D, (ekhteiarisalmas@itu.edu.tr)

Serdar Durdagi, Ph.D, (serdar.durdagi@med.bau.edu.tr)

ABSTRACT

The dopamine receptor D2 (D2R) plays an important role in the human central nervous system and is a focal target of antipsychotic agents. The previously developed $D2^{High}R$ and $D2^{Low}R$ dimeric models by our group are used to investigate the prediction of binding affinity of LY404,039 ligand and its binding mechanism within the catalytic domain. The obtained computational data using molecular dynamics (MD) simulations fits well with the experimental results. The calculated binding affinities of LY404,039 using MM/PBSA for the $D2^{High}R$ and $D2^{Low}R$ targets were -12.04 and -9.11 kcal/mol, respectively. The experimental results suggest that LY404,039 binds to the $D2^{High}R$ and $D2^{Low}R$ with 8.2 and 1640 nM binding affinities (K_i), respectively. The high binding affinity of LY404,039 in terms of binding to [^{3}H]domperidone was inhibited by the presence of guanine nucleotide, indicating an agonist action of the drug at $D2^{High}R$. The interaction analysis demonstrated that while Asp114 was among the most critical amino acids for $D2^{High}R$ binding, residues Ser193 and Ser197 were significantly more important within the binding cavity of $D2^{Low}R$. Molecular modeling analyses are extended to ensemble docking as well as structure-based pharmacophore model (E-Pharmacophore) development using the bioactive conformation of LY404,039 at the binding pocket as template and screening of small-molecule databases with derived pharmacophore models.

Keywords: Antipsychotics; Schizophrenia; Dopamine D2 Receptor; LY404,039; Molecular Modeling; MM-PBSA; Molecular Dynamics (MD) Simulations; E-Pharmacophore Modeling; Ensemble Docking

INTRODUCTION

The significant role of G-protein coupled receptors (GPCRs) in numerous human diseases motivate researchers in academia and industry to elucidate the structural and dynamical profiles as well as mechanism of action of ligands binding into the GPCR cavity spaces [1-4]. GPCRs transfer signals into the cell via conformational activation that is done by their physiological or synthetic small ligands [3,5].

So far, around 800 human GPCR genomes have been determined and divided into 5 classes: rhodopsin, secretin, adhesion, glutamate, and frizzled receptor-2. These 5 groups were also subdivided into other classes based on their amino acid sequences [6]. It is known that the rhodopsin-like receptors from class-A are among the most common GPCRs and contain around 85% of the human GPCR genomes [7]. Despite the diversity in amino acid sequences of GPCRs, these proteins share a common topology and signal transferring functionality [8-9].

Obtaining crystal structures of GPCRs are extremely challenging because of their hydrophobic soluble proprieties [10]. However, a small number of available antagonist- and agonist-bound crystal structures of GPCRs in the protein data bank (PDB) are available. The largest number of GPCR crystal structures solved refer to the active form of GPCR belongs to the β2 adrenergic receptor [11]. This conformation provides useful insight into GPCR activation as well as the coupling mechanisms of G-proteins at the cytoplasmic domain [11].

Dopamine receptor D2 (D2R) belongs to the GPCR family and although its structure is similar to that of many other GPCRs its exact structure remains to be elucidated [12-13]. Dopamine receptors (DRs) are considered essential in vertebrate central nervous system (CNS) function. It is a key target in therapies for a variety of psychotic disorders [14-19]. Growing evidence suggests that most of antipsychotic drugs bind to the binding pocket of D2Rs and inhibit the target protein with different degrees of inhibition (i.e., 60 to 80%) [15,20]. Numerous experimental and *in silico* approaches were used to investigate this receptor, which has led to a better understanding of its function and in particular the activation mechanism of the binding site [21-26]. As we discussed

above, D2R is among the hydrophobic-soluble proteins, hence elucidation of its tertiary structure has been considered a challenge [27]. Chien *et al.* [28] was the first group that was successful in deriving the inactive form of the human Dopamine receptor D3 (D3R). The modeling of D2R appears to be feasible because of the high-homology sequences between these two receptors.

In our previous studies [21-25], the structure of D2R has been estimated and validated starting from the β2 adrenergic receptor and also from the solved inactive form of the human D3R; and developed 3D models were used to investigate the influence of the activation with conformational change on the binding pocket. In these studies, the binding affinity calculations of antipsychotics in $D2^{High}R$ (active) and $D2^{Low}R$ (inactive) states were performed using dimeric and monomeric forms. The results showed that homodimerization reveals a negative cooperativity on the binding abilities of the ligands.

Herein, we focused primarily on the LY404,039 ligand, which has been used in schizophrenia targeted treatments and is considered to be a potent D2R agonist [29,30]. Using different experimental and theoretical techniques, the binding affinities of this compound to the dimeric $D2^{High}R$ and $D2^{Low}R$ states was determined and the results showed an effect of the activation process on the catalytic domain of D2R. In addition, the binding mechanism and conformational changes of the systems were investigated by molecular dynamics (MD) simulations. The data provided useful structural and dynamical information on the molecular binding profile of LY404,039 in the $D2^{High}R$ and $D2^{Low}R$-states, which allows to determine the crucial amino acids that are involved in the binding domain.

RESULTS AND DISCUSSION

The dimeric forms of $D2^{High}R$ and $D2^{Low}R$ that are modeled and validated by our group were used in MD simulations and post-processing of MD trajectories. [21-25] In this study, the binding affinity values of LY404,039 molecule at active (high) and inactive (low) states of D2R was predicted and compared with the experimental results. Moreover, a thorough conformational analysis as well as the mode of binding of the ligand at the binding pockets of $D2^{High}R$ and $D2^{Low}R$ leads to a better

understanding of the bioactive conformation of LY404,039 and crucial amino acids at the binding cavities. The conformation of the dimeric model data was in very good agreement with the data that Guo *et al*. and Lee *et al*. reported, in which the TM4 domain was determined as an important binding interface for homodimer formation and the identification of the critical amino acids involved within this domain [31,32].

Energetic Analysis of LY404,039 in Complex with $D2^{High}R$ and $D2^{Low}R$

Calculations of free energies of binding of conformational flexible biosystems are very challenging by means of MD or Monte Carlo (MC) simulations, due to an insufficient conformational sampling to obtain reliable thermodynamics. In order to bypass this limitation, all the MD trajectory frames obtained from the 100-ns MD simulations (about 10000 trajectory frames) were incorporated in the thermodynamic analysis. In the MM/PBSA analysis, not only free energy terms of LY404,039 binding to $D2^{High}R$ and $D2^{Low}R$ but also other energy related subcomponents are calculated (see Table 1 and Figure 1). Gibbs free energy differences upon LY404,039 binding to the $D2^{High}R$ and $D2^{low}R$, were estimated as -12.04 and -9.11 kcal/mol, respectively. These results suggest that the calculations were consistent with the experimental results that the LY404,039 has a higher binding affinity for $D2^{High}R$ [30].

The formation of both complexes was also accompanied by entropic penalties (values of 2.54 kcal/mol and 1.78 kcal/mol were calculated for $D2^{High}R$ and $D2^{Low}R$, respectively). This may be due to the strong polar interactions formed between the ligand and the active site amino acids and a loss of conformational degrees of freedom. The binding energy in the gas phase (ΔG_{gas}), which comprises vdW and the electrostatic components, were determined as -132.63 kcal/mol and -63.58 kcal/mol for $D2^{High}R$ and $D2^{Low}R$, respectively. The gas phase, which was used here allows to estimate the solvation free energy (ΔG_{sol}). The term of ΔE_{vdW} which contributes to the non-bonded interactions between the ligand and protein were calculated as -65.50 kcal/mol and -60.27 kcal/mol for the $D2^{High}R$ and $D2^{Low}R$ states, respectively. These terms together with the electrostatic energies indicate that the binding pockets of $D2^{High}R$ and $D2^{Low}R$ in complex with LY404,039 significantly

comprise polar and strong non-bonded interactions. This is explicitly discussed in the ligand-protein interactions analysis (see below), as in thermodynamics, where the decrease in MM energy is defined as the formation of strong binding interactions between the two compounds.

Another important thermodynamic property is the solvation free energy, which comprises polar and nonpolar subcomponents. The polar and nonpolar terms contribute to the implicit solvation within the bulk and the binding cavity, respectively. In the case of the $D2^{High}R$ and $D2^{Low}R$ forms, the solvation energies were unfavorable and they were determined as 53.65 kcal/mol and 72.00 kcal/mol, respectively. The unfavorable and positive solvation energies were reasonably expected and may be due to the high polarity nature of LY404,039 and its favorable interactions with the water molecules within the bulk. The Gibbs free energy difference decreases for the $D2^{High}R$ state to -12.04 kcal/mol with the addition of entropic term. The corresponding value for $D2^{Low}R$ form was estimated to -9.11 kcal/mol. In addition, in order to monitor the changes of the Gibbs free energy as a function of time throughout the simulation, free energy differences were calculated for each MD trajectory and results are shown in Figure 2. Although in the initial simulations, higher fluctuations in energy were observed; a significant stability was observed for the rest of the simulations. In brief, apart from entropy and solvation energy, all the energetic terms indicate favorable binding to both complexes. Also, the data are consistent with experimental results and it suggests a high affinity binding of LY404,039 to the $D2^{High}R$ forms. In addition to MM-PBSA assays, binding energies of the LY404,039 are determined by molecular docking methods. The represented protein structures from the MD trajectory frames were used as target structures in docking simulations. Figure 2 represents GOLD docking (ChemScore) and Fitness scores throughout the docking simulations which generated 1000 poses for both $D2^{High}R$ and $D2^{Low}R$ targets. The results of docking and Fitness scores for 1000 docking poses show that the LY404,039 is more selective to the high-affinity form in comparison to the low-affinity state. The results are in a satisfactory agreement with the experiments and MM-PBSA calculations. Figure 3 represents top-docking poses derived from GOLD docking simulations based on ChemScore re-scoring functions (see also Figure S1 at the

Supplementary Materials for an animation showing top-docking solutions at the $D2^{High}R$ and $D2^{Low}R$ targets). Average GOLD docking scores (ChemScore ΔG) were calculated as -3.337 and -2.454 kcal/mol for $D2^{High}R$ and $D2^{Low}R$, respectively. Corresponding values for GOLD Fitness scores were calculated as 45.839 and 38.301 for $D2^{High}R$ and $D2^{Low}R$, respectively. (A more positive value for GOLD Fitness scores indicate better fit in the binding pocket.)

Ensemble docking is performed using different conformations derived from trajectory frames throughout MD simulations in addition to single protein ligand docking. Consistent results between single protein ligand docking and ensemble docking is observed (Table 2). The RMSD matrix of ranked solutions for $D2^{High}R$ (left) and $D2^{Low}R$ (right) targets using ensemble docking simulations is also tabulated (Table 3).

Although docking scores obtained from GOLD docking protocol underestimates ligand's binding in both states of D2Rs, it demonstrated well the selectivity of the ligand toward the $D2^{High}R$ form. The docking scores of compound using other docking protocols were also calculated. For this aim, Schrodinger's Induced Fit Docking (IFD) and Quantum-Polarized Ligand Docking (QPLD) modules were used. IFD protocol is able to dock the compounds in the binding pockets, while ligands and the amino acids within the specified distance (i.e., 5 Å of the ligand) are kept flexible. Successful docking approach requires the accurate calculations and modeling of the partial atomic charges that ligand is bearing. Quantum mechanics (QM) modeling may give the highest level of docking precision when specifically the induced charge polarization of the active site of receptor is considered. For the underlying consideration regarding accuracy of docking results, QPLD is used which is based on *ab initio* charge calculations. This approach uses QSITE program for QM/MM calculations which is coupled with JAGUAR module for the QM region and the IMPACT molecular modeling code for the MM region. While IFD gives top-docking scores of -7.55 kcal/mol and -6.67 kcal/mol for $D2^{High}R$ and $D2^{Low}R$, respectively; corresponding values were found as -6.45 and -4.73 kcal/mol for QPLD. Like GOLD program, both docking protocols IFD and QPLD demonstrated well the selectivity of the ligand toward the $D2^{High}R$ form.

In addition to GOLD single and multiple-targets docking approach, MOE molecular modeling package is also used for the analysis of ligand-receptor interactions. 1000 docking poses were derived for $D2^{High}R$ and $D2^{Low}R$ targets using flexible docking approach induced fit docking (IFD). Count of residue and ligand (docking poses) interactions for backbone and sidechain atoms using

derived 1000 docking poses per each target ($D2^{High}R$ and $D2^{Low}R$) from MOE IFD docking is represented at the Figure 4. This figure allows to identify crucial amino acids in the binding pocket throughout docking simulations. The crucial amino acids for ligand binding at $D2^{High}R$ from backbone and sidechains were Val111, Ile183, Ile184, Ala185, Asn186; and Val111, Asp114, Ile183, Ile184, His393, Tyr408, and Tyr416, respectively. Corresponding amino acids at $D2^{Low}R$ from backbone and sidechains were Ser167, Asn186, Phe189, Val190; and Val111, Thr112, Val115, Leu170, Leu171, Ile184, Asn186, Phe189, Val190, Ser193, and His393, respectively.

We also evaluated crucial interactions which are occurring in three different structures to compare the consistency of used algorithms: (i) top-docking poses derived from GOLD docking simulations, (ii) results from MOE IFD docking approach and (iii) representative structures from MD simulations. Val111, Asp114, Ile184, Asn186, and His393 are common crucial amino acids in all three different approaches in $D2^{High}R$ state. These observations clearly indicate that consensus docking from different algorithms successfully predict interactions in the binding pocket.

Thr112, Asn186, and Ser193 were predicted as crucial amino acid residues for binding interactions with LY404,039 in all approaches in $D2^{Low}R$ state. His393 interacts with ligand in MOE IFD docking and representative structure from MD. Interaction between ligand and Leu170 and Leu171 were detected in both GOLD and MOE IFD docking simulations.

Competition of LY404,039 with [^{3}H]domperidone

The binding affinities of LY404,039 in the presence of [^{3}H]domperidone for the $D2^{High}R$ and $D2^{Low}R$ has been studied in our previous work and the results show that the ligand is able to inhibit the binding of [^{3}H]domperidone to D2R in a biphasic manner [30]. While the dissociation constant, K_i, of LY404,039 for $D2^{High}R$, is measured to be 8.2 nM using [^{3}H]domperidone, the corresponding value was 1640 nM for $D2^{Low}R$ [30]. The concentration to inhibit 50% of the high-affinity component of [^{3}H]domperidone binding to the $D2^{High}R$ is observed as 50 nM. This component of 15.5% for $D2^{High}R$ was eliminated in the presence of 200 μM guanylylimidodiphosphate. LY404,039 also stimulated the incorporation of [^{35}S]GTP-Γ-S into the D2R over the same range of

concentrations that inhibited the binding of [^{3}H]domperidone at D2^{High}R. In fact, the EC_{50} for this stimulating action was 80 nM, which is in general agreement with the value of 50 nM for 50% inhibition of the high-affinity component that was inhibited by LY404,039. The maximal amount of incorporation was 43% of that caused by 10 µM dopamine. The incorporation stimulated by LY404,039 was inhibited by the presence of 10 µM S-sulpiride.

Conformational Analysis

The structural and dynamical behavior of both states of D2R in complex with LY404,039 along the 100-ns classical MD simulations were studied. The data was profiled as a function of time (Figure 5). Conformational changes of the Cα atoms of both systems were measured by root-mean-square deviation (RMSD) calculations. The average RMSD of Cα atoms from the initial positions were evaluated. Mean RMSDs of the high and low forms of D2R were calculated as 1.84 and 1.78 Å, respectively. It is known that both systems fluctuate in the same range and the conformational activation does not affect the dynamics of the D2R. In addition to the protein, the conformational change as well as the diffusion of the ligand were also evaluated. For this aim, the systems were aligned with respect to the initial positions of Cα atoms and heavy atoms of ligand. The results are shown in Figure 5 and are labeled as *"ProFit"* and *"LigFit"* modes. Average RMSD values for the high and low forms of D2R were calculated as 1.37 Å and 3.07 Å, respectively. This suggests that the ligand of the low-affinity D2R revealed a higher diffusion and motility in the binding site. In contrast, the ligand in the active site of D2^{High}R was shown significant stability. The results fit well with the binding affinity calculations. The conformational changes of the ligand in the "*LigFit*" mode shows that, LY404,039 in the binding site of D2^{High}R form has less conformational degrees of freedom (0.38 Å) relative to the D2^{Low}R form (0.87 Å). Furthermore, in order to show the conformational stabilities of LY404,039 along the simulations, the RMSD data are clustered and the pairwise RMSD calculations are carried as a term of matrix by an in-house script, as shown in Figure 6. It can be understood that the ligand in the D2^{High}R form appears slightly more stable compared to the D2^{Low}R form.

LY404,039-D2R Interaction

Binding mechanisms of LY404,039 in the catalytic domains of the $D2^{High}R$ and $D2^{Low}R$ forms were evaluated throughout the MD simulations. The crucial amino acids involved in the active site of the targets and their binding interactions together with their occupancy values were determined. Figure 7 represents the fraction of interactions of the ligand to the active site amino acids of both forms. In the case of $D2^{High}R$, Val111, Asp114, Ile184, Asn186, and His393 were observed as key amino acids that play a central role in ligand stabilization via the formation of strong hydrogen bonds. In addition, Asp114 was involved in the formation of ionic bonds. Ile184 and Asn186 contributed to the water-mediated interactions, which showed that water molecules were among the most important elements in the shaping of the binding site. LY404,039 in the $D2^{Low}R$ was accommodated and stabilized via polar interactions, in which Thr112, Asn186, Ser193, and Ser197 were significantly pronounced. Interestingly, Asp114 was not determined as a conserved amino acid for the $D2^{Low}R$ form, rather Serine amino acids were observed as the crucial regions in the binding pocket. Moreover, in order to better illustrate the LY404,039 positioning within the catalytic domain of the high and low forms of D2R, 2D and 3D ligand interactions diagrams were profiled (Figures 8 and 9). The key amino acids within 5 Å of the ligand are illustrated with their occupancy values as well as the water molecules that contributed to these interactions. The 3D ligand interaction diagrams suggest that LY404,039 is accommodated well in the binding cavity of both systems. The hydrogen bond formation and the orientation of the main amino acids contributing to these interactions were also depicted.

Mutation Study

In order to determine the changes in the systems due to the Alanine mutations, the amino acids which are considered as the crucial elements in the active sites by the ligand-protein interaction assays are incorporated in the mutation study [33-35]. The results are listed in Tables 4 and 5. In the case of the $D2^{High}R$, the total predicted affinity values, which comprises *hydrogen bond*, *vdW*, *lipo*, *solv GB*, and *Coulomb* contributions, are determined to be positive for the all mutated residues.

Asp114Ala and His393Ala have a significantly pronounced effect, which may be due to the loss of strong polar interactions between the ligand and the mutated residues. Another considered term is the stability, which is described as the difference in free energy between the folded and the unfolded forms and calculated by Prime MM/GBSA. Apart from Ser197, distinct increases in energy are observed for several residues of the mutated systems, which is expected and shows the impacts of these residues in binding. The same trend is shown in the case of the total energy, by which it is found that the mutations have caused an increase in the energy of the system. Moreover, the change in the *total surface area (SASA)*, which is the sum of two polar and nonpolar terms, is calculated due to the mutation. The predicted values are all positive, which mainly demonstrates the increases at the nonpolar SASA of the mutated residues. By the considering of the low-affinity form, apart from Ser197, all the changes in affinities of the LY404,039 in the mutation system are determined to be positive, and particularly Thr112Ala and Ser193Ala have revealed significant impact of the binding energies. It is noticed that despite no strong interaction observed between Val111 and ligand, the stability value has been increased for the Val111Ala form. Expectedly, Asp114Ala could not reveal a significant change on the $D2^{Low}R$ form, but on the contrary, this mutation appears critical for the $D2^{High}R$ state because of main polar interactions which have been formed by Asp114.

Conformational Analysis of the Ligand at the Binding Pocket

Alternative conformations of small compounds commonly differ in the dihedral angles of their rotatable single bonds [36]. The torsional angle changes of LY404,039 within the binding domains of the High and Low D2R forms were measured along the simulations. These data provided information on the degree of bond rotations based on interactions with the active site amino acids. As shown in Figure 10, LY404,039 includes two main rotatable bond to which carboxyl groups were linked and are depicted by green and blue colors. These two carboxyl groups were considered crucial for giving the lowest energy conformation of the ligand at the polar binding site. Consequently, the rotations on these domains may be effective in binding of the ligand to the D2R. Based on these profiles, the rotatable bonds in the $D2^{Low}R$ were slightly flexible in comparison with

the $D2^{High}R$ form. This can be associated with interactions formed by charged Asp114 and His393 residues with the amine and carboxyl groups of the ligand, respectively. These interactions are shown in Figures 8 and 9. In summary, based on the rotatable bond data, LY404,039 in both forms, was conformationally restricted in the binding cavity.

E-Pharmacophore Modeling Studies

E-Pharmacophore modeling (structure-based pharmacophore modeling) uses advantages of both ligand- and structure-based approaches by deriving energetically optimized structure-based pharmacophore models. For this aim, representative conformers from MD simulations are used for E-pharmacophore studies. Three-sited (*DNN*) and two-sited (*NN*) hypotheses were found to be top-scored pharmacophore models for $D2^{High}R$ and $D2^{Low}R$, respectively. These main interactions were hydrogen-bond donating (labeled as "*D*") and negative-charged interactions (labeled as "*N*"), (see Figure 11). These hypotheses are then used for ligand screening from the Otava tangible (around 2500000 compounds) and Enamine databases (around 500000 compounds). The compounds that have high-fitness scores with the E-pharmacophore sites are then docked with the Glide/SP docking protocol from Schrodinger's Maestro molecular modeling package and top-scored compounds were collected. Compounds that have high docking scores and high fitness scores are shown in Figure 12.

CONCLUSION

In conclusion, dimeric models of the High and Low forms of D2R were developed and utilized to determine LY404,039 binding affinities and binding mechanisms, as well as to identify the critical amino acids that facilitate these interactions. Based on the experimental and theoretical data, LY404,039 showed greater selectivity for the $D2^{High}R$ state in comparison with the $D2^{Low}R$ state. While Asp114 was among the most critical amino acids for $D2^{High}R$, Ser193 and Ser197 were crucial for $D2^{Low}R$ binding. Molecular modeling analyses are extended to ensemble docking as well as E-Pharmacophore model development using the bioactive conformation of LY404,039 at the binding pocket as template and screening of small-molecule databases with these derived pharmacophore models.

MATERIALS AND METHODS

[^{3}H]Domperidone and [^{3}H](+)PHNO Binding to Dopamine Receptors

The effect of LY404,039 on dopamine D2 and D3 receptors was measured in our previous report [30] by competition with [^{3}H]Domperidone and with [^{3}H](+)PHNO on human cloned D2 Long receptors (in CHO cells; Liu et al., 2000), on rat cloned dopamine D3 receptors (in CHO cells), and on rat homogenized striata, using methods previously reported [37-39]. The effect of LY404,039 on the incorporation of [^{35}S]GTP-Γ-S was measured as previously described [39].

Ligand Preparation

The 2D structure of the LY404,039 was manually sketched and minimized by a force field method (OPLS 2005) [40] in order to obtain the low energy 3D structure of the ligand. Protonation of the ligand was then assigned at a physiological pH (pH = 7.4) by Epik [41] module implemented in the Schrodinger molecular modeling package. Atomic electrostatic potential (ESP) derived charges were calculated by a semi-empirical method, Austin Model 1 (AM1) [42]. In order to obtain the lowest energy conformation of the ligand, a conformational search method was used, in which all possible conformations were generated by a systematic MC method.

Homology Modeling

$D2^{High}R$ and $D2^{Low}R$ conformers were modeled using the full active and inactive β2-adrenergic receptor structures. The crystal structures of the templates were retrieved from PDB IDs: 3SN6, 3D4S [11,43]. Dimeric forms of the models were constructed based on configuration of the rhodopsin oligomer (PDB ID: 1N3M) [44], in which the TM4 in both monomers played a major role in dimerization stability, as suggested by Guo *et al.* and Lee *et al.* [31,32]. The details of the homology modeling were described in our previous studies [22], in which the methods and parameters that used for the loop modeling and the TM domains and as well as relaxation and homodimerization of the systems were completely explained.

Molecular Docking

Molecular docking studies were performed via GOLD 5.3.0 [45] and MOE [46].

GOLD: GOLD docking protocol possesses a genetic algorithm that works with four related steps: (i) a population of potential binding poses at a defined binding pocket is set up at random; (ii) each member of the population is encoded as a "*chromosome*", which contains information about the mapping of protein−ligand interactions; (iii) each *chromosome* is assigned a fitness score based on its predicted binding affinity, and the *chromosomes* within the population are ranked according to fitness; and (iv) the population of *chromosomes* is iteratively optimized. In this study, the following genetic algorithm parameters were used (populations size, 1000; selection pressure, 1.1; number of islands, 5; migrate, 10; mutate, 95; crossover, 95; niche size, 2; and number of operations, 107000). Default cutoff values of 2.5 Å (dH-X) for hydrogen bonds and 4.0 Å for van der Waals distance were employed. Search efficiency was set to its maximum value (200%) in order to increase the reliability of the docking results. In the GOLD docking algorithm, active site residues (Val111, Thr112, Asp114, Ile184, Asn186, Ser193, Ser197 and His393) for both receptor states were selected according to their ligand interaction map of the representative complexes derived from MD trajectories. The defined residues were treated as flexible and their side chains were rotated in 10° increments and scanned over 360°. In GOLD algorithm, two docking scoring functions were combined: GoldScore (for docking) and ChemScore (for re-scoring).

Ensemble docking with multi-target procedure for both states of D2 receptor is also used besides the single-target molecular docking. Representative structures of D2 receptors with 13 diverse conformations were derived from MD trajectories and all were used for ensemble docking studies. The genetic algorithm settings in this process were used as the same as the single-target docking mentioned above.

MOE (v.2014.09): Two different docking scores were utilized in order to evaluate the predicted binding free energy of the ligands to these receptors: (i) London dG and (ii) GBVI/WSA dG (Generalized-Born Volume Integral/Weighted Surface Area dG). Triangle Matcher was chosen as the ligand placement methodology. MMFF94x force field is used to refine the free energy of binding in the second refinement step. 1000 poses were generated in each re-scoring steps.

MD Simulations

The systems were embedded into a dipalmitoylphosphatidylcholine (DPPC) membrane bilayer, and then solvated in an orthorhombic box with layers of explicit TIP3P water molecules of 15 Å thickness. All the atomistic MD simulations were carried out using the Desmond code. [47] The interactions between the atoms were calculated by OPLS 2005 force field. The particle-mesh Ewald method [48] was used to calculate the long-range electrostatic interactions. A cut-off radius of 12.0 Å was used for van der Waals and Coulombic interactions. Nose−Hoover thermostat [49] and Martyna−Tobias−Klein protocols [50] were used to maintain the temperature and pressure of the systems at 310 K and 1.01325 bar, respectively. Time step of the simulation was assigned as 2.0 fs. All the atoms were minimized for a maximum of 5000 iterations, and a convergence threshold of 1 kcal mol^{-1} $Å^{-1}$ was implemented. Afterwards, the protein and water atoms were relaxed using step-wise methods, in which the systems were gradually equilibrated. Finally, 100-ns MD simulations was carried out for each system.

Molecular Mechanics Poisson–Boltzmann Surface Area (MM/PBSA)

Binding free energy predictions have been proven as a feasible approach for studying biological systems, such as protein-protein and protein-ligand interactions [51]. MM/PBSA is a straightforward method that predicts ligand binding free energy in complex with biological macromolecules [52]. The MM/PBSA method that has been implemented to determine the energy terms, is profiled in Figure 13, in which LY404,039 together with D2R in both gas, explicit, implicit solvation models, and as well as hydrophobic membrane bilayer are simulated.

Binding free energies are achieved by subtracting the individual free energies of the receptor and ligand from the free energy of the complex structure as given in equation 1:

$$\Delta G_{bind} = G_{complex} - (G_{protein} + G_{ligand}) \qquad (1)$$

The energetic calculations were performed using *MMPBSA.py*, [52] Python code of AmberTools16 [53]. The complete details of the method and the relevant thermodynamic equations were described in our previous study [23].

AUTHOR INFORMATION

Corresponding Authors

***E-mail:** ekhteiarisalmas@itu.edu.tr

***E-mail:** serdar.durdagi@med.bau.edu.tr

Notes

The authors declare no competing financial interest.

REFERENCES

1. Römpler, H., Stäubert, C., Thor, D., Schulz, A., Hofreiter, M., and Schöneberg, T. (2007) G protein-coupled time travel: evolutionary aspects of GPCR research. *Mol. Interv. 7*, 17–25.
2. Wise, A., Gearing, K., and Rees, S. (2002) Target validation of G-protein coupled receptors. *Drug Discov. Today*.
3. Stevens, R. C., Cherezov, V., Katritch, V., Abagyan, R., Kuhn, P., Rosen, H., and Wüthrich, K. (2013) The GPCR Network: a large-scale collaboration to determine human GPCR structure and function. *Nat. Rev. Drug Discov. 12*, 25–34.
4. Rajagopal, S., Rajagopal, K., and Lefkowitz, R. J. (2010) Teaching old receptors new tricks: biasing seven-transmembrane receptors. *Nat. Rev. Drug Discov. 9*, 373–86.
5. Saunders, B. *et al.* The molecule pages database. *Nucleic Acids Res.* 36, (2008).
6. Foord, S. M. *et al.* International Union of Pharmacology. XLVI. G Protein-Coupled Receptor List. *Pharmacol. Rev.* 57, 279–288 (2005).
7. Joost, P. & Methner, A. Phylogenetic analysis of 277 human G-protein-coupled receptors as a tool for the prediction of orphan receptor ligands. *Genome Biol.* 3, RESEARCH0063 (2002).
8. Shonberg, J. *et al.* Biased Agonism at G Protein-Coupled Receptors: The Promise and the Challenges-A Medicinal Chemistry Perspective. *Med. Res. Rev.* 34, 1286–1330 (2014).
9. Trzaskowski, B. *et al.* Action of Molecular Switches in GPCRs - Theoretical and Experimental Studies. *Curr. Med. Chem.* 19, 1090–1109 (2012).
10. Shonberg, J., Kling, R. C., Gmeiner, P. & L??ber, S. GPCR crystal structures: Medicinal chemistry in the pocket. *Bioorganic Med. Chem.* 23, 3880–3906 (2014).
11. Rasmussen, S. G. F. *et al.* Crystal structure of the β2 adrenergic receptor-Gs protein complex. *Nature* 477, 549–55 (2011).
12. Seeman, Chau-Wong, M., Tedesco, J. & Wong, K. Brain receptors for antipsychotic drugs and dopamine: direct binding assays. *Proc. Natl. Acad. Sci. U. S. A.* 72, 4376–80 (1975).
13. Seeman, P. & Van Tol, H. H. M. Dopamine receptor pharmacology. *Trends Pharmacol. Sci.* 15, 264–270 (1994).
14. Seeman, P. & Tallerico, T. Rapid release of antipsychotic drugs from dopamine D2 receptors: An explanation for low receptor occupancy and early clinical relapse upon withdrawal of clozapine or quetiapine. *Am. J. Psychiatry* 156, 876–884 (1999).
15. Seeman, P. Targeting the dopamine D2 receptor in schizophrenia. *Expert Opin. Ther. Targets* 10, 515–31 (2006).
16. Seeman, P. An update of fast-off dopamine D2 atypical antipsychotics [4]. *Am. J. Psychiatry* 162, 1984–1985 (2005).
17. Seeman, P. Are dopamine D2 receptors out of control in psychosis? *Prog. Neuropsychopharmacol. Biol. Psychiatry* 46, 146–52 (2013).
18. Seeman, P. All Roads to Schizophrenia Lead to Dopamine Supersensitivity and Elevated Dopamine D2High Receptors. *CNS Neurosci. Ther.* 17, 118–132 (2011).

19. Seeman, P. Dopamine D2High receptors measured ex vivo are elevated in amphetamine-sensitized animals. *Synapse* 63, 186–192 (2009).
20. Farde, L. *et al.* Positron Emission Tomographic Analysis of Central D1-Dopamine and D2-Dopamine Receptor Occupancy in Patients Treated with Classical Neuroleptics and Clozapine - Relation to Extrapyramidal Side-Effects. *Arch. Gen. Psychiatry* 49, 538–544 (1992).
21. Salmas, R. E., Yurtsever, M., Stein, M. & Durdagi, S. Modeling and protein engineering studies of active and inactive states of human dopamine D2 receptor (D2R) and investigation of drug/receptor interactions. *Mol. Divers.* 19, 321–332 (2015).
22. Durdagi, S., Salmas, R. E., Stein, M., Yurtsever, M. & Seeman, P. Binding Interactions of Dopamine and Apomorphine in D2High and D2Low States of Human Dopamine D2 Receptor Using Computational and Experimental Techniques. *ACS Chem Neurosci* 7, 185–195 (2016).
23. Ekhteiari Salmas, R., Seeman, P., Aksoydan, B., Stein, M., Yurtsever, M., and Durdagi, S. (2017) Biological Insights of the Dopaminergic Stabilizer ACR16 at the Binding Pocket of Dopamine D2 Receptor. *ACS Chem. Neurosci.* acschemneuro.6b00396.
24. Salmas, R. E., Yurtsever, M., and Durdagi, S. (2016) Atomistic molecular dynamics simulations of typical and atypical antipsychotic drugs at the dopamine D2 receptor (D2R) elucidates their inhibition mechanism. *J. Biomol. Struct. Dyn.* 1–17.
25. Salmas, R. E., Stein, M., Yurtsever, M., Seeman, P., Erol, I., Mestanoglu, M., and Durdagi, S. (2016) The signaling pathway of dopamine D2 receptor (D2R) activation using normal mode analysis (NMA) and the construction of pharmacophore models for D2R ligands. *J. Biomol. Struct. Dyn. 1102*, 1–9.
26. Seeman, P. & Tallerico, T. Antipsychotic drugs which elicit little or no parkinsonism bind more loosely than dopamine to brain D2 receptors, yet occupy high levels of these receptors. *Mol. Psychiatry* 3, 123–134 (1998).
27. Ghosh, E., Kumari, P., Jaiman, D. & Shukla, A. K. Methodological advances: the unsung heroes of the GPCR structural revolution. *Nat Rev Mol Cell Biol* 16, 69–81 (2015).
28. Chien, E. Y. T. *et al.* Structure of the human dopamine D3 receptor in complex with a D2/D3 selective antagonist. *Science* 330, 1091–5 (2010).
29. Patil, S. T., Zhang, L., Martenyi, F., Lowe, S. L., Jackson, K. A., Andreev, B. V, Avedisova, A. S., Bardenstein, L. M., Gurovich, I. Y., Morozova, M. A., Mosolov, S. N., Neznanov, N. G., Reznik, A. M., Smulevich, A. B., Tochilov, V. A., Johnson, B. G., Monn, J. A., and Schoepp, D. D. (2007) Activation of mGlu2/3 receptors as a new approach to treat schizophrenia: a randomized Phase 2 clinical trial. *Nat Med 13*, 1102–1107.
30. Seeman, P., and Guan, H. C. (2009) Glutamate agonist LY404,039 for treating schizophrenia has affinity for the dopamine D2High receptor. *Synapse 63*, 935–939.
31. Guo, W., Shi, L., Filizola, M., Weinstein, H., and Javitch, J. a. (2005) Crosstalk in G protein-coupled receptors: changes at the transmembrane homodimer interface determine activation. *Proc. Natl. Acad. Sci. U. S. A. 102*, 17495–17500.
32. Lee, S. P., O'Dowd, B. F., Rajaram, R. D., Nguyen, T., and George, S. R. (2003) D2 dopamine receptor homodimerization is mediated by multiple sites of interaction, including an intermolecular interaction involving transmembrane domain 4. *Biochemistry 42*, 11023–11031.
33. Zhu, K., Day, T., Warshaviak, D., Murrett, C., Friesner, R., and Pearlman, D. (2014) Antibody structure determination using a combination of homology modeling, energy-based refinement, and loop prediction. *Proteins Struct. Funct. Bioinforma. 82*, 1646–1655.
34. Salam, N. K., Adzhigirey, M., Sherman, W., Pearlman, D. A., and Thirumalai, D. (2014) Structure-based approach to the prediction of disulfide bonds in proteins, in *Protein Engineering, Design and Selection*, pp 365–374.

35. Beard, H., Cholleti, A., Pearlman, D., Sherman, W., and Loving, K. A. (2013) Applying physics-based scoring to calculate free energies of binding for single amino acid mutations in protein-protein complexes. *PLoS One 8*.
36. Brameld, K. A., Kuhn, B., Reuter, D. C. & Stahl, M. Small molecule conformational preferences derived from crystal structure data. A medicinal chemistry focused analysis. *J. Chem. Inf. Model.* 48, 1–24 (2008).
37. Seeman, P. (2007) Antiparkinson therapeutic potencies correlate with their affinities at dopamine D2High receptors. *Synapse 61*, 1013–1018.
38. Seeman, P. (2008) Dopamine D2High receptors moderately elevated by bifeprunox and aripiprazole. *Synapse 62*, 902–908.
39. Seeman, P., and Guan, H. C. (2008) Phencyclidine and glutamate agonist LY379268 stimulate dopamine D2 high receptors: D2 basis for schizophrenia. *Synapse 62*, 819–828.
40. Siu, S. W. I., Pluhackova, K. & Böckmann, R. A. Optimization of the OPLS-AA force field for long hydrocarbons. *J. Chem. Theory Comput.* 8, 1459–1470 (2012).
41. Shelley, J. C. *et al.* Epik: A software program for pKa prediction and protonation state generation for drug-like molecules. *J. Comput. Aided. Mol. Des.* 21, 681–691 (2007).
42. Dewar, M. J. S., Zoebisch, E. G., Healy, E. F. & Stewart, J. J. P. Development and use of quantum mechanical molecular models. 76. AM1: a new general purpose quantum mechanical molecular model. *J. Am. Chem. Soc.* 107, 3902–3909 (1985).
43. Hanson, M. A. *et al.* A Specific Cholesterol Binding Site Is Established by the 2.8 Å Structure of the Human beta2-Adrenergic Receptor. *Structure* 16, 897–905 (2008).
44. Fotiadis, D. *et al.* Structure of the rhodopsin dimer: a working model for G-protein-coupled receptors. *Curr. Opin. Struct. Biol.* 16, 252–259 (2006).
45. Verdonk, M. L., Cole, J. C., Hartshorn, M. J., Murray, C. W., and Taylor, R. D. (2003) Improved protein-ligand docking using GOLD. *Proteins Struct. Funct. Genet. 52*, 609–623.
46. Vilar et al, Vilar, S., Cozza, G., and Moro, S. (2008) Medicinal chemistry and the molecular operating environment (MOE): application of QSAR and molecular docking to drug discovery. *Curr. Top. Med. Chem. 8*, 1555–1572.
47. Desmond Bowers, K., Chow, E., Xu, H., Dror, R., Eastwood, M., Gregersen, B., Klepeis, J., Kolossvary, I., Moraes, M., Sacerdoti, F., Salmon, J., Shan, Y., and Shaw, D. (2006) Scalable Algorithms for Molecular Dynamics Simulations on Commodity Clusters. Proceed- ings of the ACM/IEEE Conference on Supercomputing (SC06), Tampa, Florida, November 11−17.
48. Essmann, U. *et al.* A smooth particle mesh Ewald method. *J Chem Phys* 103, 8577–8593 (1995).
49. Hoover, W. G. Canonical dynamics: Equilibrium phase-space distributions. *Phys. Rev. A* 31, 1695–1697 (1985).
50. Martyna, G. J., Tobias, D. J. & Klein, M. L. Constant pressure molecular dynamics algorithms. *J. Chem. Phys.* 101, 4177 (1994).
51. Leach, A. (2001) Molecular modelling: principles and applications (2nd Edition), Prentice Hall, Upper Saddle River, NJ.
52. Miller, B. R. *et al.* MMPBSA.py: An efficient program for end-state free energy calculations. *J. Chem. Theory Comput.* 8, 3314–3321 (2012).
53. D.A. Case, R.M. Betz, W. Botello-Smith, D.S. Cerutti, T.E. Cheatham, III, T.A. Darden, R.E. Duke, T.J. Giese, H. Gohlke, A.W. Goetz, N. Homeyer, S. Izadi, P. Janowski, J. Kaus, A. Kovalenko, T.S. Lee, S. LeGrand, P. Li, C. Lin, T. Luchko, R. Luo, B. Madej, D. Mermelstein, K.M. Merz, G. Monard, H. Nguyen, H.T. Nguyen, I. Omelyan, A. Onufriev, D.R. Roe, A. Roitberg, C. Sagui, C.L. Simmerling, J. Swails, R.C. Walker, J. Wang, R.M. Wolf, X. Wu, L. Xiao, D.M. York and P.A. Kollman (2016), AMBER 2016, University of California, San Francisco.
54. Kyte, J., and Doolittle, R. F. (1982) A simple method for displaying the hydropathic character of a protein. *J. Mol. Biol. 157*, 105–132.

TABLES

Table 1. Energetic analysis of LY404,039 in complexes with the dimeric $D2^{High}R$ and $D2^{Low}R$, as obtained by MM-PBSA method.

Energy term	**Mean value (kcal/mol) ± SEM[a]**	
	$D2^{high}R$–$D2^{high}R$	**$D2^{low}R$–$D2^{low}R$**
ΔE_{vdw}	-65.50 ± 0.28	-60.27 ± 0.20
ΔE_{elec}	-106.13 ± 2.41	-33.30 ± 2.17
ΔE_{MM}	-132.63 ± 2.21	-63.58 ± 2.01
ΔG_{PB}	159.78 ± 1.50	105.30 ± 1.36
ΔG_{NP}	-2.72 ± 0.00	-2.61 ± 0.00
ΔG_{solv}	157.05 ± 1.50	102.68 ± 1.35
$\Delta G_{elec(tot)}$	53.65	72.00
ΔH	-14.58 ± 1.06	-10.89 ± 1.14
$-T\Delta S$	2.54	1.78
$\Delta G_{MM\text{-}PBSA}$	-12.04 ± 1.06	-9.11 ± 1.14
$\Delta G_{Exp.}$	-11.09	-7.93
[a]Standard error of the mean (SEM)		

Table 2. GOLD Ensemble docking analysis for ligand binding at $D2^{High}R$ (left) and $D2^{Low}R$ (right) targets.

High				**Low**			
GA Run	Protein	Fitness	ChemScore ΔG (kcal/mol)	GA Run	Protein	Fitness	ChemScore ΔG (kcal/mol)
19	5	69.10	-3.820	8	7	45.68	-1.918
17	7	65.22	-3.821	11	7	44.81	-1.806
16	4	59.50	-4.706	19	5	44.45	-2.342
7	9	58.88	-4.050	17	9	43.58	-2.499
15	3	58.13	-2.989	16	11	42.89	-2.486
8	5	57.54	-4.972	13	13	42.14	-1.898
20	8	57.38	-2.308	12	13	41.79	-1.970
10	5	56.73	-4.592	9	12	41.69	-2.462
13	2	55.02	-1.648	10	11	41.61	-2.438
11	6	54.61	-3.040	20	6	41.42	-1.839
4	9	54.50	-3.787	14	3	41.06	-1.904
2	2	54.37	-3.511	7	12	40.12	-2.403
12	9	53.98	-3.614	5	11	39.98	-3.112
1	8	53.86	-3.615	6	10	39.97	-2.170
18	9	52.99	-3.263	15	9	39.28	-1.802
6	6	52.40	-2.815	1	5	39.04	-2.273
3	5	52.12	-4.508	2	2	39.02	-2.389
5	4	52.03	-3.795	3	11	38.98	-1.754
9	7	51.99	-2.988	4	7	38.83	-1.805
14	11	50.25	-3.222	18	12	37.92	-2.289
	Average	**56.03**	**-3.553**		**Average**	**41.21**	**-2.178**

Table 3. RMSD Matrix of ranked solutions for $D2^{High}R$ (left) and $D2^{Low}R$ (right) targets using ensemble docking.

RMSD Matrix of RANKED solutions

	2	3	4	5	6	7	8	9	10	11	12	13	14	15	16	17	18	19	20
1	4.5	4.6	4.4	2.4	4.5	4.5	3.3	4.3	2.4	4.2	3.6	4.5	4.7	5.5	3.7	5.0	4.8	4.4	6.1
2		4.1	3.6	3.9	4.2	4.2	3.6	4.9	3.4	4.2	3.3	4.0	0.9	4.3	3.3	4.5	1.5	3.6	5.6
3			4.7	4.6	4.6	1.1	4.4	3.7	3.6	5.3	4.8	1.2	4.0	4.3	2.1	4.5	3.9	4.8	5.6
4				4.1	3.2	4.5	2.7	5.8	3.3	2.8	1.8	4.6	3.4	4.2	4.2	4.2	3.4	0.7	6.0
5					4.9	4.3	3.1	4.1	1.9	4.4	2.8	4.1	4.1	5.2	3.6	5.2	4.7	4.3	5.4
6						4.9	3.4	4.5	4.4	1.7	3.5	4.9	4.4	3.4	4.6	3.1	3.9	2.7	5.4
7							4.3	4.0	3.3	5.3	4.6	1.0	4.0	4.4	2.2	4.6	4.1	4.6	5.7
8								4.8	2.8	3.4	2.4	4.3	3.7	4.8	3.8	4.7	3.9	2.7	5.0
9									4.5	4.7	5.1	3.8	5.1	3.8	4.2	3.8	5.4	5.7	4.5
10										4.2	2.6	3.2	3.4	4.8	2.3	4.8	3.7	3.5	5.6
11											2.7	5.3	4.3	3.5	5.0	3.1	4.2	2.4	5.8
12												4.5	3.2	4.3	4.1	4.3	3.6	1.9	5.6
13													3.8	4.3	1.8	4.7	4.1	4.7	5.5
14														4.2	3.4	4.5	1.5	3.4	5.9
15															4.5	1.3	4.4	4.1	5.0
16																4.8	3.4	4.3	5.6
17																	4.4	4.0	5.2
18																		3.2	6.2
19																			5.9

RMSD Matrix of RANKED solutions

	1	2	3	4	5	6	7	8	9	10	11	12	13	14	15	16	17	18	19
1	4.6	4.5	0.7	3.0	2.2	4.6	5.7	2.5	4.3	4.9	4.1	2.9	4.5	4.4	4.4	5.2	5.2	3.9	4.0
2		5.9	4.4	5.6	4.2	1.5	5.3	5.2	4.4	2.1	5.7	5.4	2.7	1.2	5.9	3.2	5.5	4.5	5.5
3			4.6	3.1	4.9	6.4	4.0	3.2	5.4	5.5	3.1	3.0	6.2	5.8	0.4	5.0	4.4	4.6	3.1
4				3.2	1.7	4.3	5.9	2.8	4.4	4.7	4.5	3.0	4.2	4.2	4.6	5.3	5.5	4.0	4.2
5					3.7	6.1	5.0	0.8	4.8	5.8	3.8	0.4	6.0	5.4	3.1	5.6	4.7	4.5	3.8
6						4.1	6.4	3.1	4.1	4.8	5.3	3.4	4.2	4.0	5.0	5.5	6.1	4.2	5.0
7							5.8	5.6	5.0	2.5	6.2	5.9	1.6	2.0	6.4	4.0	5.9	4.5	5.9
8								5.0	5.7	4.4	3.8	5.0	5.8	5.3	4.0	3.5	2.9	4.1	4.0
9									4.3	5.4	3.7	0.6	5.7	5.0	3.2	5.3	4.7	4.3	3.8
10										4.7	4.8	4.6	5.7	4.5	5.5	4.5	5.4	4.8	5.7
11											5.0	5.6	2.9	2.0	5.5	1.8	5.0	4.0	4.8
12												3.7	6.1	5.5	3.0	4.2	4.2	4.1	3.6
13													5.8	5.2	3.1	5.4	4.7	4.4	3.8
14														2.9	6.1	4.5	5.9	4.4	5.7
15															5.8	3.1	5.7	4.4	5.2
16																5.0	4.3	4.6	3.0
17																	4.3	4.4	4.5
18																		5.2	4.0
19																			4.5

Table 4. Mutation properties of the important amino acids of the $D2^{High}R$ form. *ΔSASA (total)*, change in total surface area because of the mutation. *ΔAffinity*, change in binding affinity of the LY404,039, to the mutated D2R. (A negative value means that the mutant D2R binds better than the wild form); *ΔHydropathy*, Change in hydrophobic or hydrophilic nature of the mutated residue, as described in the Kyte-Doolittle scale [54]. A positive value shows a more hydrophobic amino acid and a negative value indicates a less hydrophobic amino acid in the mutant form. *ΔStability*, Change in the stability of the system due to the mutation, predicted by the Prime energy function using an implicit solvent. The stability is defined as the difference in free energy between the folded and the unfolded forms. A negative value indicates that the mutant system is in a more stable state than the wild system.

Δ (Change)	**Val111Ala**	**Thr112Ala**	**Asp114Ala**	**Ile184Ala**	**Asn186Ala**	**Ser193Ala**	**Ser197Ala**	**His393Ala**
Stability	13.81	6.01	1.97	13.05	3.32	2.86	-0.33	10.19
SASA (total)	0.04	17.84	5.95	30.89	35.56	1.21	0.19	23.93
Affinity H-bond	0	0	1.1	0	0	0	0	1.2
Affinity vdW	0.53	0.28	0.93	1.79	0.69	0.05	0.03	0.52
Hydropathy	0	0.16	0.09	-0.46	0.98	0.06	0.01	0.87
Affinity Lipo	0.66	0.08	0	1.83	0	0	0	0.27
Affinity Solv GB	-0.11	0.18	8.97	-0.26	-0.83	1.27	1.04	-30.07
Affinity Coulomb	-0.02	-0.37	-3.18	0.05	0.58	-0.43	-0.88	35.92
Energy (total)	5.75	9.35	47.73	1.36	44.05	4.41	1.6	22.05
Affinity (total)	1.06	0.17	7.82	3.42	0.44	0.89	0.18	7.84

Table 5. Mutation properties of the important amino acids of the $D2^{Low}R$ form.

Δ (Change)	Val111Ala	Thr112Ala	Asp114Ala	Ile184Ala	Asn186Ala	Ser193Ala	Ser197Ala	His393Ala
Stability	7.62	-0.92	2.72	12.64	1.01	-5.83	2.16	2.95
SASA (total)	-4.14	0.19	17.6	33.93	9.53	-0.57	2.4	20.22
Affinity H-bond	0	0.23	0	0	0.26	0.88	0	0.02
Affinity vdW	0.27	-0.6	0.04	0.65	0.42	-0.27	0.23	1.06
Hydropathy	-0.5	0.01	0.31	-0.34	0.96	-0.04	0.01	1.08
Affinity Lipo	0.23	1.36	0	0.38	0.02	0.02	0.01	0.07
Affinity Solv GB	-0.13	-1.4	0.42	-0.09	-3	-1.04	1	0.57
Affinity Coulomb	-0.04	5.87	-0.28	-0.04	4.94	5.88	-1.39	0.1
Energy (total)	-1.17	7.71	40.84	-1.56	43.94	0.31	3.75	10.55
Affinity (total)	0.33	5.46	0.18	0.9	2.63	5.47	-0.15	1.83

FIGURES

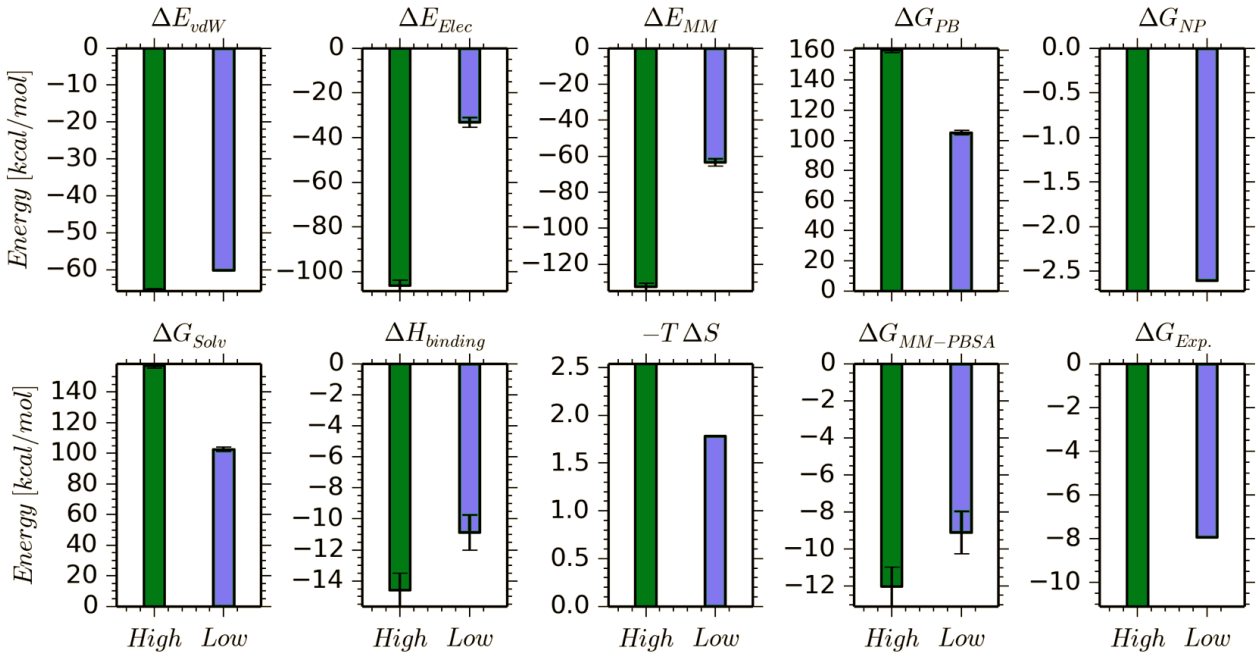

Figure 1. MM-PBSA results of LY404,039 in complexes with the dimeric $D2^{High}R$ and $D2^{Low}R$. (Green and pale blue bars show results for high and low states, respectively).

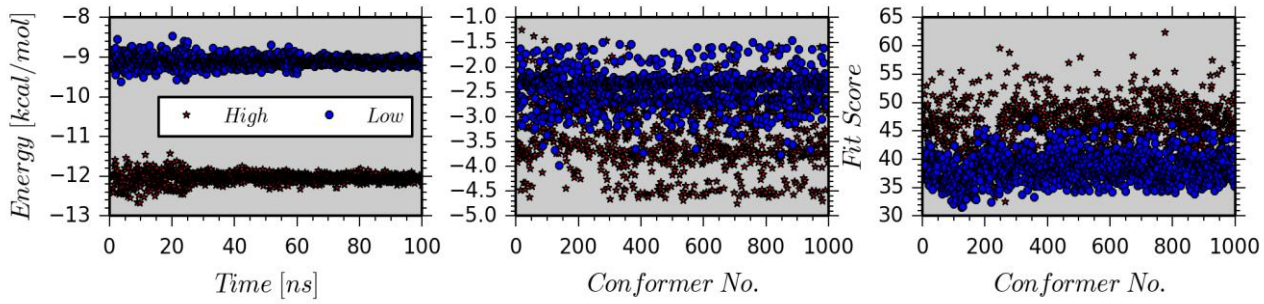

Figure 2. $\Delta G_{MM\text{-}PBSA}$ (left), GOLD docking scores (medium), and Fitness scores (right) of LY404,039 in complex with high and low forms of D2R are determined as a function of time and docking pose numbers. Average GOLD docking scores (ChemScore ΔG) were calculated as -3.337 and 2.454 kcal/mol for $D2^{High}R$ and $D2^{Low}R$, respectively. Corresponding values for GOLD Fitness scores were calculated as 45.839 and 38.301 for $D2^{High}R$ and $D2^{Low}R$, respectively. (A more positive value for GOLD Fitness scores indicate better fit in the binding pocket)

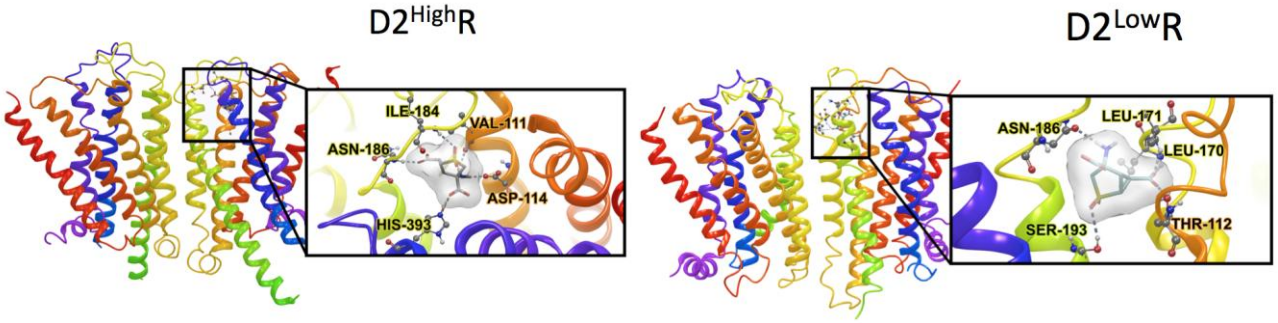

Figure 3. Top-docking poses derived from GOLD docking simulations using 1000 solutions for each target.

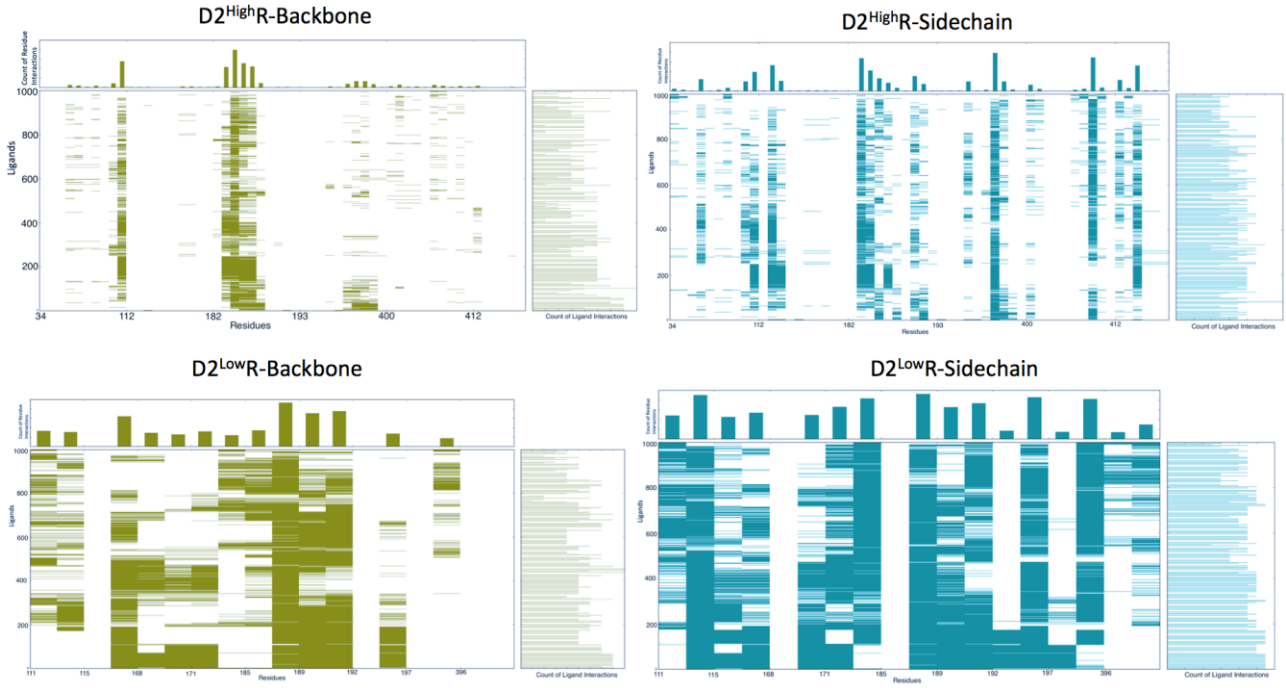

Figure 4. Count of residue and ligand (docking poses) interactions for backbone (left) and sidechain atoms (right) using derived 1000 docking poses per each target ($D2^{High}R$ and $D2^{Low}R$) from MOE IFD docking.

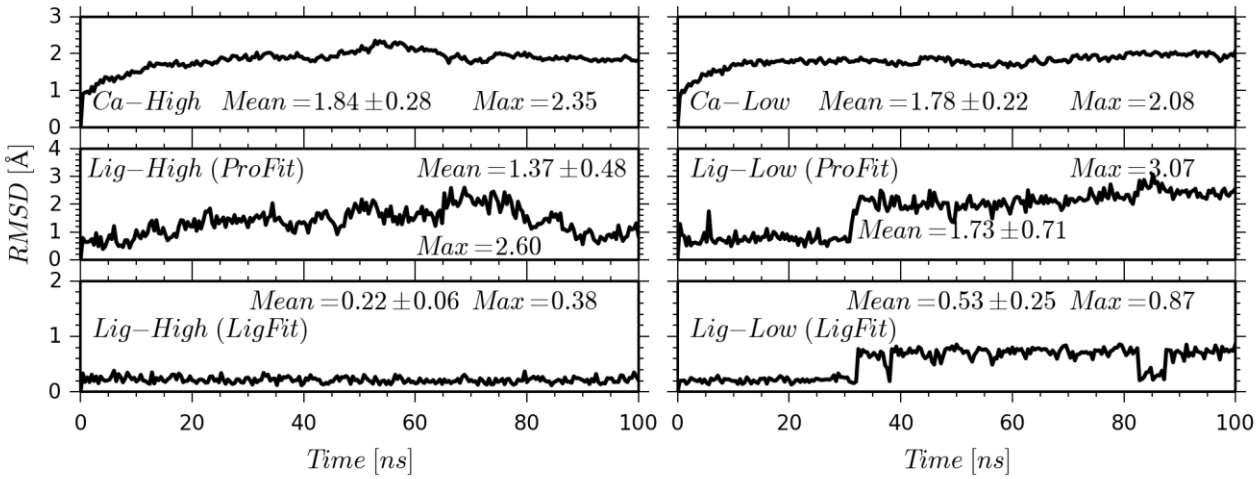

Figure 5. Conformational changes of LY404,039 and D2^{high}R and D2^{low}R atoms relative to their start positions are evaluated as a function of time. “ProFit” and ”LigFit” correspond to the modes when the systems are aligned on Ca atoms and ligand atoms, respectively.

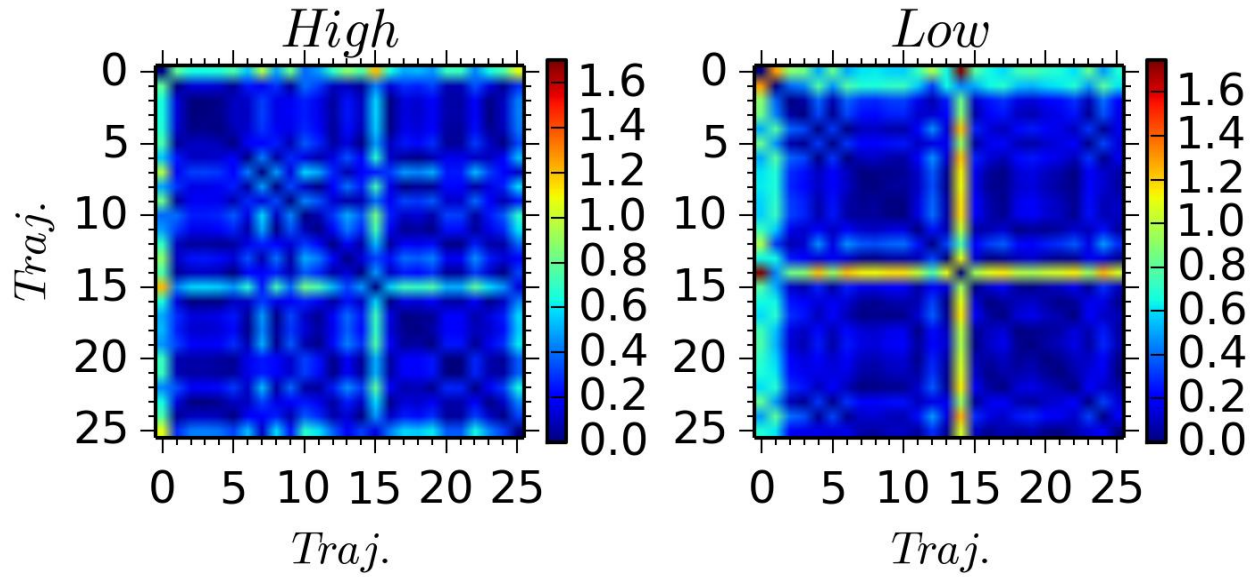

Figure 6. Pair-wise RMSD analysis of heavy atoms of the LY404,039 in the high- and low-affinity forms of D2R. The calculations and profiling of the matrices were performed by an in-house script.

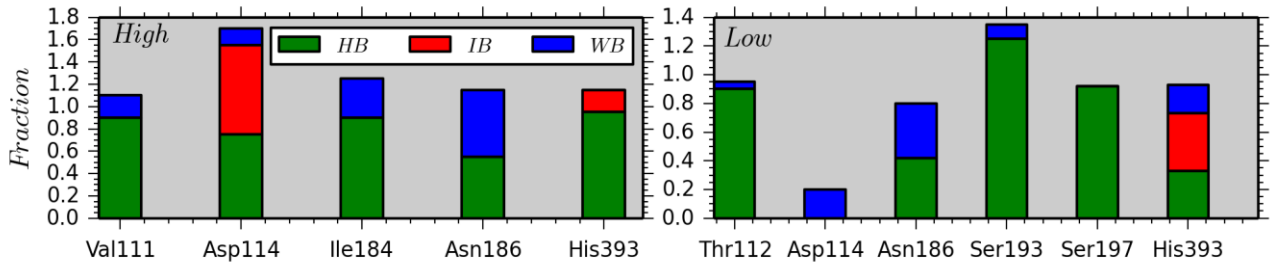

Figure 7. Per-residue interaction analysis of LY404,039 in the catalytic domains of $D2^{High}R$ and $D2^{Low}R$ along MD simulations. (While HB represents hydrogen bonding, IB and WB correspond for ionic interactions and water bridges between LY404,039 and the active site amino acids.) Occupancy values of the interactions are calculated as *y*-scale.

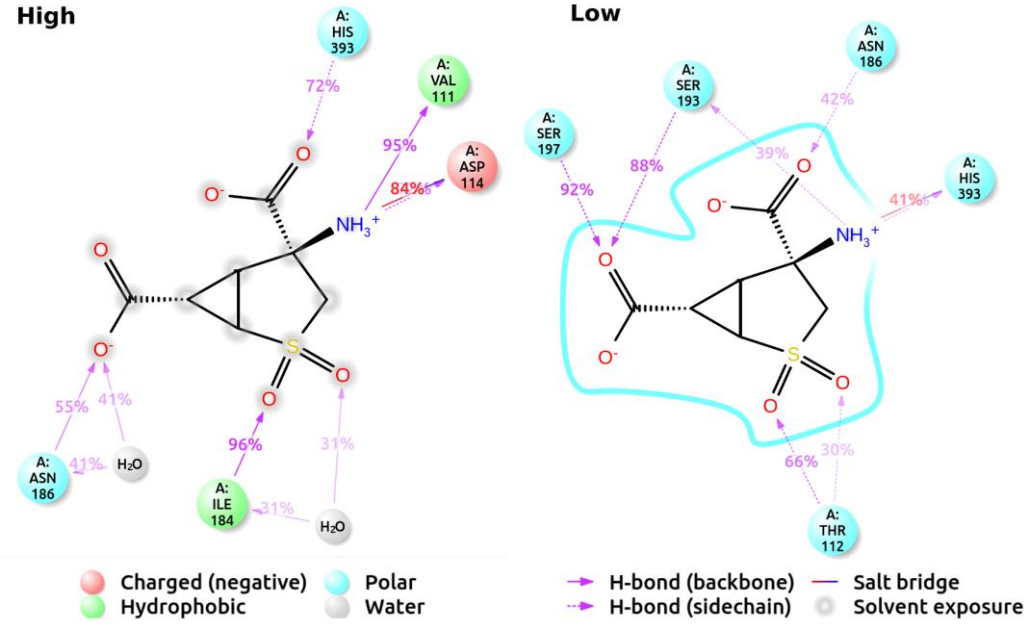

Figure 8. 2D ligand interaction diagrams of LY404,039 in complex with $D2^{High}R$ and $D2^{Low}R$ are depicted. The occupancy interactions between the ligand and active site amino acids are calculated for the individual amino acids.

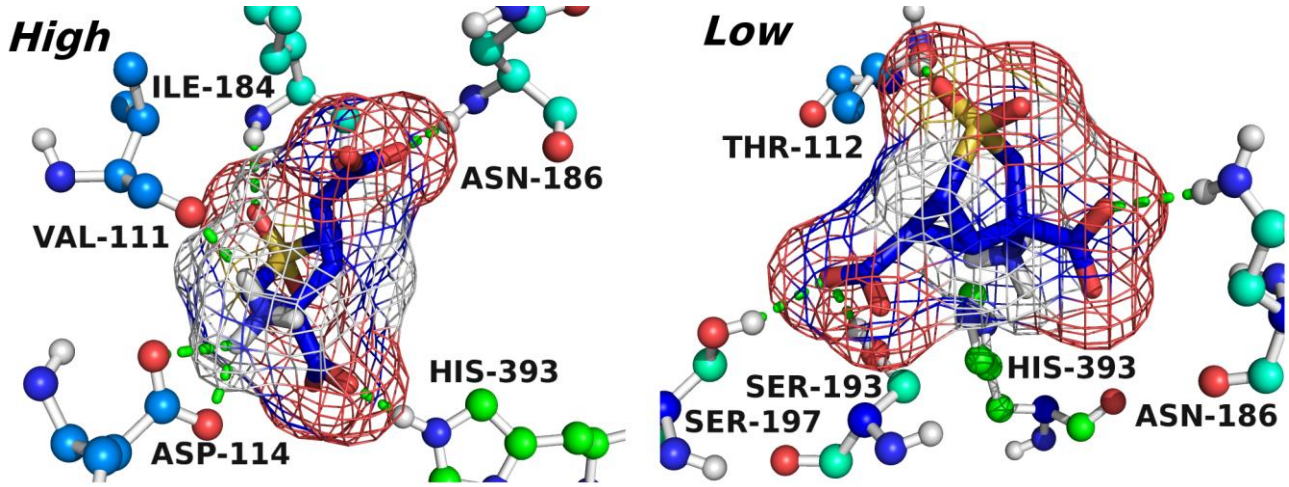

Figure 9. 3D ligand binding interactions of LY404,039 positioning within the binding pockets of the High and Low forms of D2R is shown for the representative structure from MD simulations.

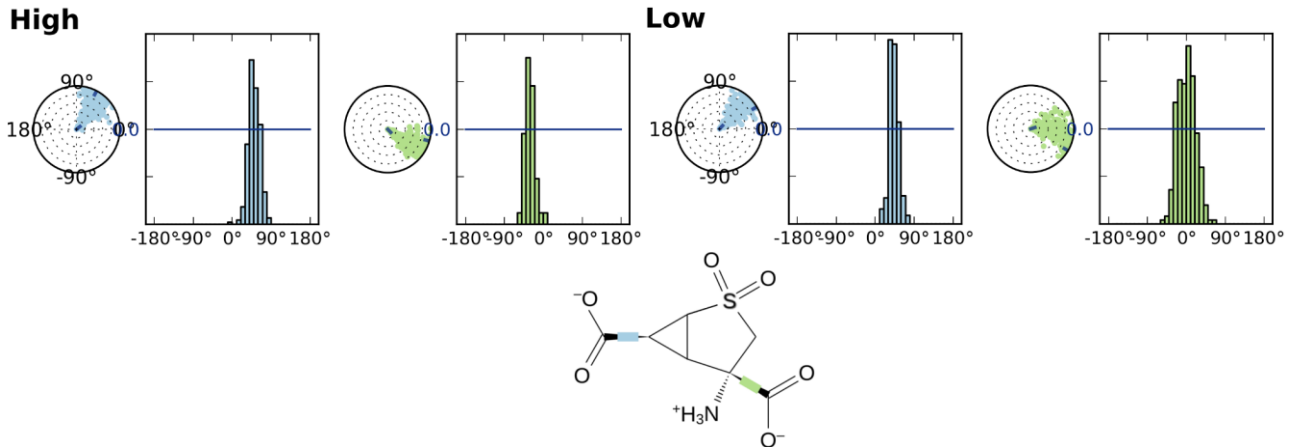

Figure 10. Rotatable bond changes of LY404,039 in the binding domain of $D2^{high}R$ and $D2^{low}R$ during MD simulations represent the conformational flexibilities of the ligand. The two rotatable bonds are associated to carboxyl groups, as depicted in the figure. The first rotatable bond (blue) has comparably similar dynamics in both forms, but as expected, for the second bond (green), the $D2^{High}R$ shows a more rigidity in comparison with the $D2^{Low}R$.

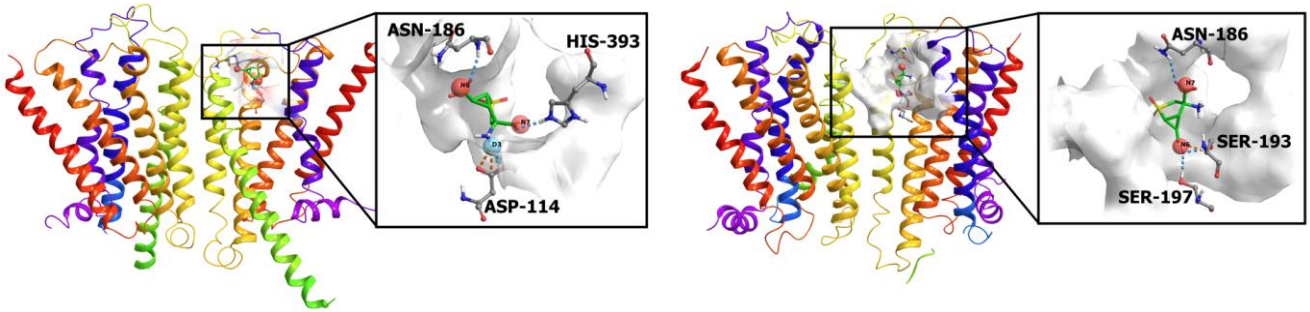

Figure 11. E-Pharmacophore sites at D2^{High}R and D2^{Low}R binding pockets. The main interactions were hydrogen-bond donating (labeled as "D") and negative-charged interactions (labeled as "N") at the derived pharmacophore models.

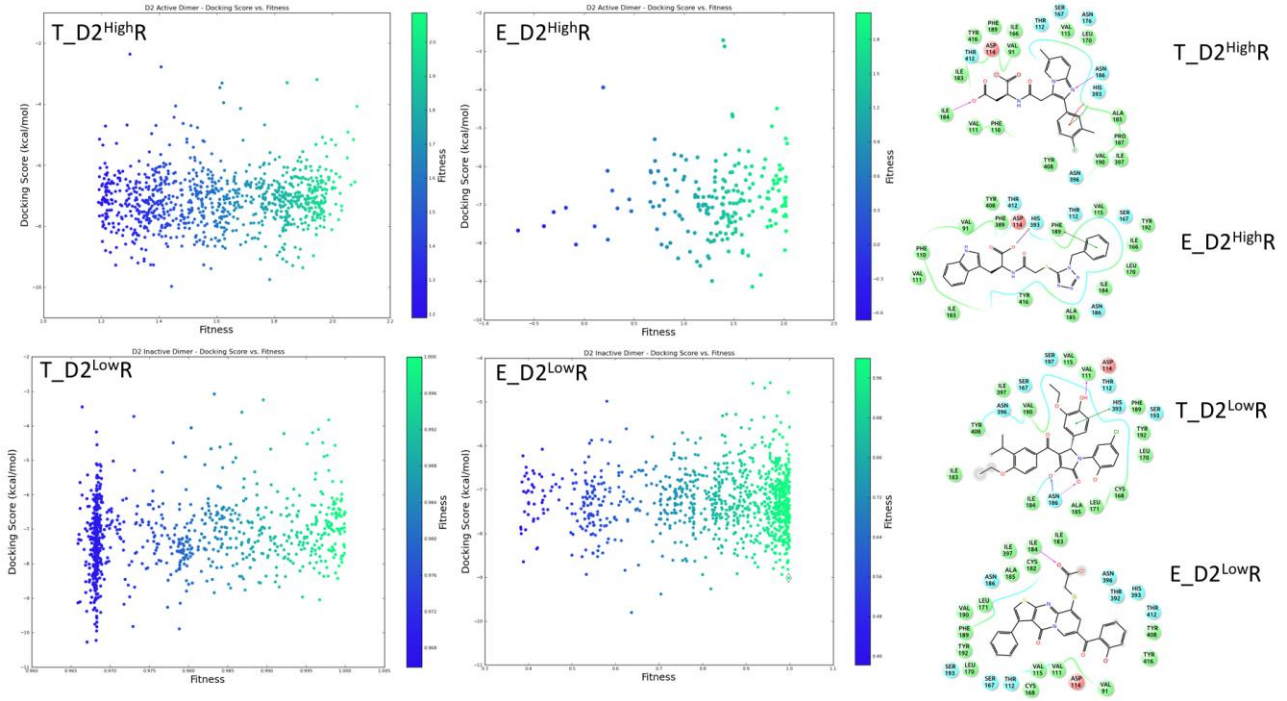

Figure 12. Around 500000 compounds from the Enamine small-molecules database (E) and around 2500000 molecules from Otava tangible database (T) are screened against derived pharmacophore models and top-1000 compounds that have high Fitness scores with these sites are then docked at the D2Rs binding pocket using Glide/SP (standard precision). Compounds that show high docking scores as well as high fitness scores are shown in the figure.

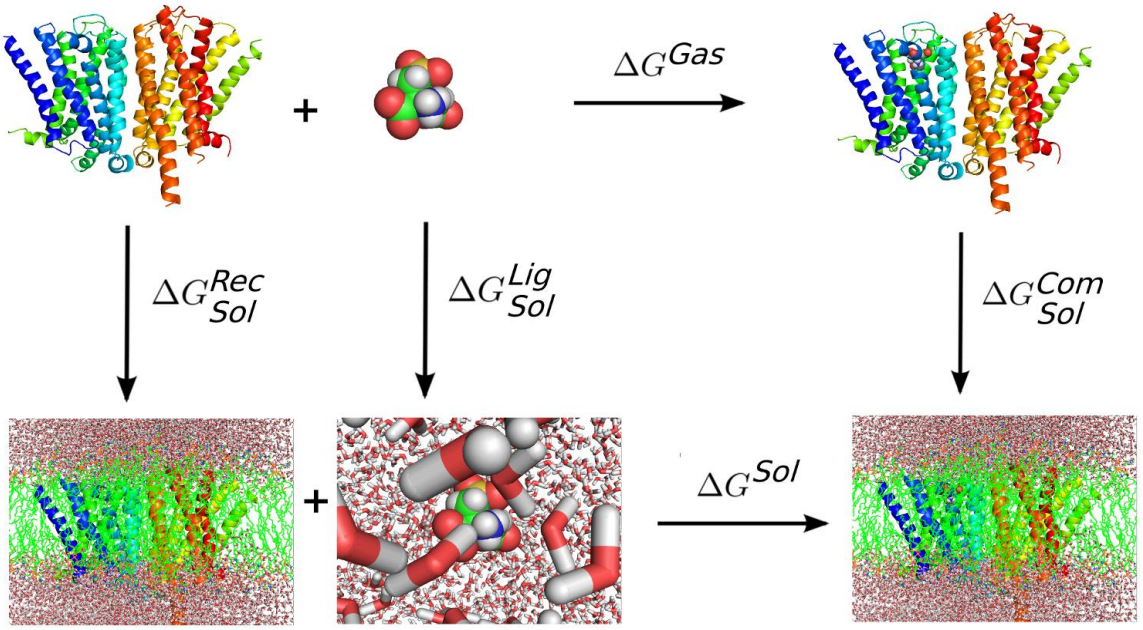

Figure 13. A schematic view of the MM-PBSA method was applied to determine the energetic terms. The LY404,039 ligand and D2R were simulated in different implicit and explicit environments.